J Mater Sci: Mater Electron
DOI 10.1007/s10854-015-3707-7

REVIEW

High temperature dielectric ceramics: a review of temperature-stable high-permittivity perovskites

A. Zeb[1] · **S. J. Milne**[1]

Received: 17 June 2015 / Accepted: 26 August 2015

Abstract Recent developments are reviewed in the search for dielectric ceramics which can operate at temperatures >200 °C, well above the limit of existing high volumetric efficiency capacitor materials. Compositional systems based on lead-free relaxor dielectrics with mixed cation site occupancy on the perovskite lattice are summarised, and properties compared. As a consequence of increased dielectric peak broadening and shifts to peak temperatures, properties can be engineered such that a plateau in relative permittivity–temperature response (ε_r–T) is obtained, giving a ±15 %, or better, consistency in ε_r over a wide temperature range. Materials with extended upper temperature limits of 300, 400 and indeed 500 °C are grouped in this article according to the parent component of the solid solution, for example $BaTiO_3$ and $Na_{0.5}Bi_{0.5}TiO_3$. Challenges are highlighted in achieving a lower working temperature of −55 °C, whilst also extending the upper temperature limit of stable ε_r to ≥300 °C, and achieving high-permittivity and low values of dielectric loss tangent, tan δ. Summary tables and diagrams are used to help compare values of ε_r, tan δ, and temperature ranges of stability for different materials.

1 Introduction

This review presents a perspective on recent research into lead-free dielectric ceramics with high and stable relative permittivity, ε_r, to temperatures ≫200 °C, well-beyond the operating limit of traditional high ε_r (Class II) dielectrics based on ferroelectric $BaTiO_3$.

The search for new and improved capacitor materials is driven by the growing demands of power electronics, where heat dissipation is an issue, and for electronics operating in harsh environments. New types of capacitor would find applications in the conversion and control of electrical energy, for example the integration of renewable energy sources with the grid, and inverters for electric and hybrid vehicles. Examples of harsh environment electronics include distributed control and sensing systems in aviation and aerospace, where electronic controls are placed close to the engine, at temperatures of 200–300 °C. This reduces interconnections, saving hundreds of kilograms of aircraft weight and increasing the reliability of the system [1, 2]. The move to mechatronics in the automotive sector requires sensing and control electronics to operate close to heat sources greater than 200 °C, whilst temperature ranges for combustion sensing are 200–300 °C, and for exhaust sensing ≥500 °C [3]. Down-hole drilling in the oil and gas industries uses electronics and sensors to steer the drilling equipment and monitor its health: the geothermal gradient is ≥25 °C/km, and in the past, drilling operations only reached temperatures of 150–175 °C, but advancing technology has made it feasible for the oil industry to drill deeper, requiring electronics that can operate reliably at higher temperatures [1, 3].

The lack of reliable high temperature, high volumetric efficiency capacitor materials, has curtailed growth in high temperature electronics [4]. Hence there is a growing awareness of the importance of research targeting the discovery and development of new, Class II robust dielectric materials. Advances in other key aspects of high temperature electronic systems, namely semiconductor and packaging materials, have resulted in components that can sustain prolonged exposure at 200–300 °C. Indeed, silicon

✉ S. J. Milne
s.j.milne@leeds.ac.uk

[1] School of Chemical and Process Engineering, University of Leeds, Leeds LS2 9JT, UK

Published online: 24 September 2015

carbide and gallium nitride wide band-gap semiconductors have been demonstrated to 300–500 °C [5, 6]. Likewise interconnects and packaging can cope with temperatures >200 °C. By contrast, commercial dielectrics, based on ferroelectric $BaTiO_3$ are restricted to below 200 °C. Moreover, polymer, glass or tantalum dielectrics are also generally specified only to ~200 °C. Lead-containing dielectric ceramics operate to ~200–250 °C but their future use is uncertain due to environmental legislation [7, 8]. Major advances have already been made in low-permittivity Class 1 dielectric ceramics; Kemet Electronics have pioneered C0G base-metal-electrode multilayer capacitors with remarkably stable performance to 200 °C and above, but these materials are not designed for high energy storage density applications [3, 9].

Given existing limitations, the development of improved, device-quality Class II high temperature, high storage density dielectrics with stable performance over wide temperature ranges to ≥300 °C would be transformative, and open up new opportunities in energy generation and transmission, the low carbon economy, and control and sensing electronics in aerospace, aviation and automotive industries.

The Electronic Industries Alliance categorises Class II capacitors according to: lower operating temperature; upper operating temperature; level of stability in capacitance—as described in Table 1. The code X7R, for example, represents dielectrics specified from −55 to 125 °C with variability in capacitance of within ±15 %. This level of performance is achieved through doping ferroelectric $BaTiO_3$, with Co, Nb or other elements, to develop core–shell segregated grain structures which result in a smearing of the Curie peak at the ferroelectric-paraelectric transition temperature, T_c which occurs at ~130 °C in unmodified $BaTiO_3$. Other chemical modifications to $BaTiO_3$ extend the upper limit to 175 °C (X9R).

Numerous complex ceramic solid solution systems have been reported which display frequency dependent, broad ε_r–T peaks characteristic of a relaxor dielectric, and over narrow compositional ranges a ε_r–T plateau develops, extending to well above 200 °C. These materials are referred to as 'temperature-stable relaxor dielectrics', and offer promise for developing new Class II capacitor materials which can operate to much higher temperatures than traditional X7R–X9R ferroelectric-based dielectrics. In a classic relaxor such as lead magnesium niobate, $Pb(Mg_{1/3}Nb_{2/3})O_3$, the ε_r–T response exhibits broad frequency-dependent ε_r peaks at a temperature denoted T_m [10–12]. Structural models to explain the dielectric properties of relaxors are generally based on the effect of mixed valence occupancy in disrupting long-range (ferroelectric) polar order, resulting in polar nanoregions, as in B-site disorder on the ABO_3 perovskite structure of $Pb(Mg_{1/3}Nb_{2/3})O_3$ [13, 14]. The broad frequency dependent ε_r peak characteristic of a relaxor, Fig. 1, is thought to originate from temperature-dependent changes in the length scales and coupling dynamics of polar nanoregions.

An example is shown in Fig. 2 of how a diffuse ε_r relaxor peak can be further broadened and suppressed by additional cation substitutions on A and B sites of the ABO_3 lattice to develop a temperature-insensitive ε_r (T) plateau. The region of stable ε_r (defined as $\varepsilon_{r\ mid} \pm 15$ % or better) generally has a lower temperature limit slightly below the original T_m and an upper limit at the onset of sharp increases to dielectric loss (or electronic conduction).

The mechanisms leading to conversion of a classic relaxor to a temperature-stable relaxor lie outside the scope of this review. Indeed little is known as to the chemical or structural origins, other than lose empirical correlations between mixed site occupancy levels and the suppression of the ε_r peak. It may be that lattice scale heterogeneity

Table 1 EIA standard specification codes for class II types dielectrics for capacitor applications

1st letter		Numeric		2nd letter	
Symbol	Low temperature limit (°C)	Symbol	High temperature limit (°C)	Symbol	Maximum % variation in capacitance
Z	+10	4	+65	A	±1.0
Y	−30	5	+85	B	±1.5
X	−55	6	+105	C	±2.2
		7	+125	D	±3.3
		8	+150	E	±4.7
		9	+175	F	±7.5
				P	±10.0
				R	±15.0
				S	±22.0

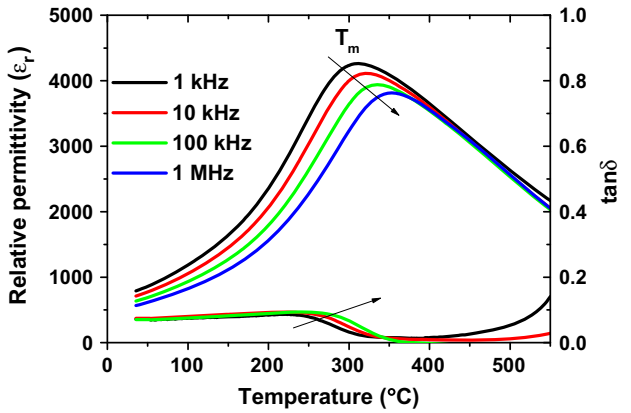

Fig. 1 Frequency dependent ε_r peak, and tan δ dispersion, in a relaxor dielectric $0.9K_{0.5}Bi_{0.5}TiO_3$–$0.1Ba(Zr_{0.2}Ti_{0.8})O_3$ [15] (Color figure online)

supresses the normal changes in polar structure/coupling on cooling from the Burns temperature through the ergodic region [17], as in the example of $Ba_{0.8}Ca_{0.2}TiO_3$–$Bi(Mg_{0.5}Ti_{0.5})O_3$, where the anticipated A site ions are Ba^{2+}, Ca^{2+}, Bi^{3+} and the B sites, Mg^{2+}, Ti^{4+} (Ca^{2+}) [16]. Unlike ferroelectric based X7R dielectrics, strong evidence of core–shell segregation is not visible in electron micrographs of high temperature analogues; it may be a factor but if so involve more subtle compositional variations and/or involve chemical heterogeneity over shorter length scales. Future work to examine the possibility that clustering of specific cations occurs on a nanoscale, over dimensions of a few unit cells, could give valuable insights into factors that may contribute to fluctuations in local electric and elastic fields that moderate and supress normal relaxor ε_r (T) behaviour.

This review focusses on basic dielectric parameters of ceramic compositions that offer promise as high volumetric efficiency Class II capacitor materials. Relative permittivity ε_r, loss tangent tan δ and electrical resistivity versus temperature are described and compared (ε_r and tan δ are generally quoted for measurements at 1 kHz). Where available, data on RC time constant and energy storage density are also presented. These basic parameters in themselves do not confirm that a particular material is a suitable capacitor material. However they do enable the most promising dielectric materials to be screened and selected for follow on capacitor-grade evaluation trials. The latter would require fabrication of ceramic layers and multi-layers for testing of insulation resistance, dielectric breakdown strength, voltage coefficient, energy density, power density, dc degradation etc., involving highly accelerated life testing.

The value and temperature range of stability in relative permittivity is a helpful basic comparison point to assess materials being considered as high temperature dielectrics. Claims of a wide working temperature range based solely

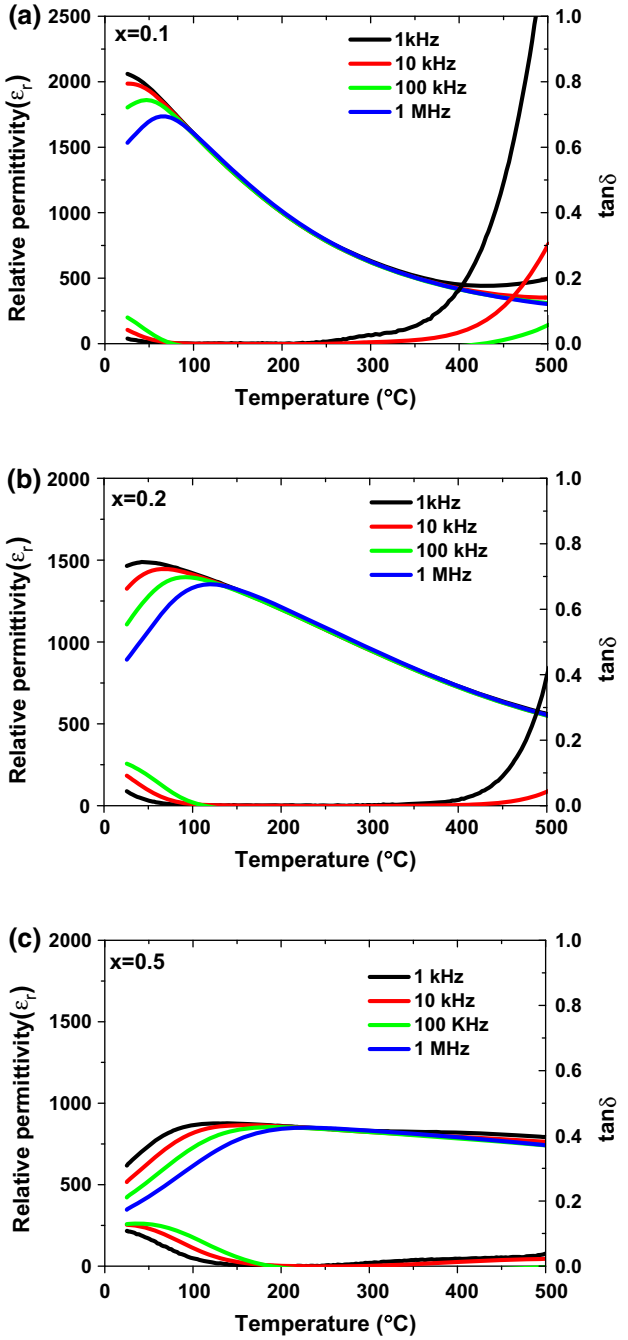

Fig. 2 Progression in ε_r–T response from **a**, **b** normal relaxor to **c** a temperature-stable relaxor by increasing the level of mixed cation substitution for the system, $(1 - x)Ba_{0.8}Ca_{0.2}TiO_3$–$xBi(Mg_{0.5}Ti_{0.5})O_3$: **a** x = 0.1; **b** x = 0.2; **c** x = 0.5 [16] (Color figure online)

on temperature range of stable ε_r may be misleading, should dielectric losses or electrical conductivity rise above acceptable limits. A reasonable benchmark for 'low dielectric loss' is taken in this review to correspond to tan δ ≤ 0.02 (5). It is also important to scrutinise if a reported wide temperature range of stable ε_r refers to overlapping temperature ranges of multiple compositions

in a solid solution series: it should of course only refer to one specific material i.e. one solid solution composition.

As mentioned above, the two main categories of perovskite ceramics in which temperature-stable dielectric relaxor characteristics with consistency in $\varepsilon_r \pm 15$ % over wide ranges of temperature extending to 200–500 °C are based on solid solutions involving $BaTiO_3$ and/or $Na_{0.5}Bi_{0.5}TiO_3$ as end-members. These materials, and selected examples of other compositional families, are presented and compared in the following sections. Tables 1 and 2 summarise dielectric properties, resistivities and RC time constants.

2 $BaTiO_3$-based materials

2.1 $BaTiO_3$–$BiScO_3$

The $BiScO_3$ end-member has a high Curie temperature (~450 °C) but can only be prepared at high pressures and temperatures (~6 GPa, ~1100 °C) [18, 19]. Ogihara et al. [20] Penn State University, demonstrated weakly coupled relaxor behaviour in the binary system $(1 - x)BaTiO_3$–$xBiScO_3$ [BT–BS] prepared with 3 mol% excess Bi_2O_3. The Curie peak at ~130 °C became diffuse as the $BiScO_3$ content increased to x = 0.02BS. At x = 0.05BS an additional, frequency dependent peak appeared at lower temperatures. These dielectric properties were associated with a core–shell microstructure: the shell regions of the grains were enriched in $BiScO_3$ and were considered to be responsible for the lower temperature frequency dependent dielectric anomaly. A single, very diffuse relaxor ε_r–T response occurred for compositions around x = 0.2BS: this gave rise to near-stable ε_r values, 800–1000 over a wide temperature range [20]. Similar behaviour had previously been observed in thin film samples [21]. For x = 0.3 bulk ceramics, values of $\varepsilon_r \sim 1000$ were recorded from temperatures of 0 to 300 °C, with high electrical resistivity, $\sim 10^{12}$ Ω cm at 250 °C. The energy density of pellets and tape-cast thick films of these x = 0.3 samples was investigated: a 15 µm dielectric layer had a room-temperature energy density of 6.1 J/cm^3 at a dc bias field of 730 kV/cm, just below the breakdown field. Stable energy densities of 2.3 J/cm^3 for composition x = 0.3 were observed for temperatures up to 300 °C (at bias fields ~30–40 kV/cm) [20].

2.2 $BaTiO_3$–$Bi(Mg_{0.5}Ti_{0.5})O_3$

The solid solution between $BaTiO_3$ and $Bi(Mg_{0.5}Ti_{0.5})O_3$, [(1 − x)BT–xBMT] has been studied by a number of research groups. Wada et al. [22] focussed on the system's piezoelectric properties, but noted a changeover from

Table 2 Summary of selected perovskites high temperature dielectrics with wide temperature ranges of stable relative permittivity (within ±15 %)

Material system	$\varepsilon_{r\ mid}$ (T range, °C) 1 kHz	T range (°C) tan δ ≤ 0.02 (1 kHz)	ρ (Ω m) at T (°C)	RC (s) at T(°C)
$0.7BaTiO_3$–$0.3BiScO_3$ [20]	1000 ± 15 % (0–300)	50–400	–	–
$0.5BaTiO_3$–$0.5Bi(Mg_{0.5}Ti_{0.5})O_3$ [23]	2400 ± 15 % (167–400)	238–400 (100 kHz)	–	–
$0.5Ba_{0.8}Ca_{0.2}TiO_3$–$0.5Bi(Mg_{0.5}Ti_{0.5})O_3$ [16]	800 ± 10 % (45–550)	(100–400)	1.6×10^9 (300 °C)	14.8 (300 °C)
$0.45Ba_{0.8}Ca_{0.2}TiO_3$–$0.55Bi(Mg_{0.5}Ti_{0.5})O_3$ [17]	950 ± 15 % (70–600)	160–550	10^9 (300 °C)	10.4 (300 °C)
$0.8BaTiO_3$–$0.2Bi(Zn_{0.5}Ti_{0.5})O_3$ (Ba-deficient [33]	1150 ± 15 % (100–350)	tan δ ~ 0.05 (100–460)	5.78×10^7 (335 °C)	1.47 (335 °C)
$0.7Ba_{0.8}Ca_{0.2}TiO_3$–$0.3Bi(Zn_{0.5}Ti_{0.5})O_3$ [39]	1030 ± 15 % (25–425)	85–460	10^8 (300 °C)	–
$0.5BaTiO_3$–0.25BZT–0.25BS (Ba-deficient) [37]	1100 ± 15 % (80–500)	~100–450	4.1×10^7 (335 °C)	0.44 (335 °C)
$0.45Ba_{0.8}Ca_{0.2}TiO_3$–$0.35Bi(Mg_{0.5}Ti_{0.5})O_3$ –0.2$NaNbO_3$ [17]	600 ± 15 % (−70 to +500)	−20–400	5.2×10^8 (300 °C)	4.00 (300 °C)
$0.7Na_{0.5}Bi_{0.5}TiO_3$–$0.3NaNbO_3$ [46, 47]	>500 ± 15 % (−80–200)	−80 to +150	–	–
$0.9Na_{0.5}Bi_{0.5}TiO_3$–$0.1KTaO_3$ [46, 47]	>2500 ± 15 % (80–340)	tan δ ~ 0.05 (80–300)	–	–
$0.82(0.94Na_{0.5}Bi_{0.5}TiO_3$–$0.06BaTiO_3)$–$0.18K_{0.5}Na_{0.5}NbO_3$ [49]	2151 ± 10 % (43–319)	tan δ ≤ 0.025 (50–300)	10^8 (300 °C)	1.13 (300 °C)
$0.85[0.6Na_{0.5}Bi_{0.5}TiO_3$–$0.4K_{0.5}Bi_{0.5}TiO_3]$–$0.15K_{0.5}Na_{0.5}NbO_3$ [50]	2167 ± 10 % (54–400)	~100–250	$\sim 10^5$ (300 °C)	0.042 (300 °C)
$0.8[0.82(0.94Na_{0.5}Bi_{0.5}TiO_3$–$0.06BaTiO_3)$–$0.18K_{0.5}Na_{0.5}NbO_3]$–$0.2CaZrO_3$ [51]	467 ± 15 % (−69 to +468)	–	$\sim 10^8$ (300 °C)	1.07 (300 °C)

ferroelectric to relaxor characteristics occurred at 0.1 BMT [22]. A plot of ε_r–T at 1 MHz showed a very diffuse dielectric response for compositions 0.2BMT and 0.3BMT, with ε_r-values of 600–1000 at temperatures from approximately 25 to 400 °C. Dielectric loss tangent at 100 Hz was in the range 0.05–0.1.

Zhang et al. [23] provided a detailed account of the temperature stability of dielectric properties. Compositions x = 0.5BMT and 0.6BMT displayed a plateau in ε_r–T response: for x = 0.5, values of $\varepsilon_r \sim 2400 \pm 15$ % (1 kHz) were observed for temperatures 167–400 °C, with tan δ < 0.02 (100 kHz) for temperatures 238–400 °C. For x = 0.4, $\varepsilon_r \sim 2200 \pm 15$ % at temperatures of 175–400 °C; low losses occurred over most of this temperature range, with tan δ ≤ 0.02 from 197 to 400 °C (at 100 kHz).

A plot of ε_r–T for the (1 − x)BT–xBMT composition x = 0.5BMT fabricated in our laboratory is shown in Fig. 3, values of $\varepsilon_{r\ mid} = 2100 \pm 15$ % extended from 150 to 400 °C, in general agreement with literature data [23], but ε_r is slightly lower than published values, possibly due to differences in ceramic density. Values of tan δ were ≤0.02 (100 kHz) from 270 to 550 °C, and ≤0.02 at 1 kHz for the narrow temperatures range 230–300 °C.

Choi et al. [24] investigated (1 − x)BT–xBMT bulk ceramics and multilayer capacitors (20 × 129 μm layers) [24]. They found the solubility limit of BMT to occur around x = 0.4–0.5. Highly diffuse relaxor-like behaviour was observed for compositions x = 0.1–0.4. Different compositions displayed distinctive temperature ranges of stable ε_r values, depending on the T_m for each specific composition, however temperature ranges over which ε_r varied within ±15 % were not commented upon in detail.

Xiong et al., examined the effect of Nb_2O_5 and Co_2O_3 co-dopants on the properties of (1 − x)BT–xBMT: similar dopants are incorporated into BT to develop core–shell structures and X7R temperature-stable performance [25–27]. These authors reported that compositions x = 0.15BMT doped with 2 wt% Nb_2O_5 produced an $\varepsilon_r \sim 1000 \pm 15$ % over the temperature range −55 to +155 °C: tan δ = 0.09 at room temperature. Microstructures were presented to investigate possible core–shell characteristics.

2.3 $Ba_{0.8}Ca_{0.2}TiO_3$–$Bi(Mg_{0.5}Ti_{0.5})O_3$

The beneficial effect of Ca-modified $BaTiO_3$ in solid solution with $Bi(Mg_{0.5}Ti_{0.5})O_3$ was highlighted at the University of Leeds by Zeb and Milne [16]. Incorporation of Ca^{2+} into $BaTiO_3$ extends the temperature range of the tetragonal perovskite phase [28]. Some of the best high temperature dielectrics with low dielectric losses over wide temperature ranges are found in this system, Fig. 4a. The initial report of (1 − x)$Ba_{0.8}Ca_{0.2}TiO_3$–x$Bi(Mg_{0.5}Ti_{0.5})O_3$ indicated $\varepsilon_r = 800 \pm 10$ % from 45 to 550 °C, with tan δ ≤ 0.025 over the temperature range 100–430 °C for x = 0.5BMT [16]. For a slightly higher BMT content, x = 0.55BMT the dielectric properties were superior to 0.5BMT, with $\varepsilon_{r\ mid} = 1000 \pm 15$ % from 80 to 500 °C and tan δ ≤ 0.02 from 160 to 500 °C, Fig. 4a [17, 29].

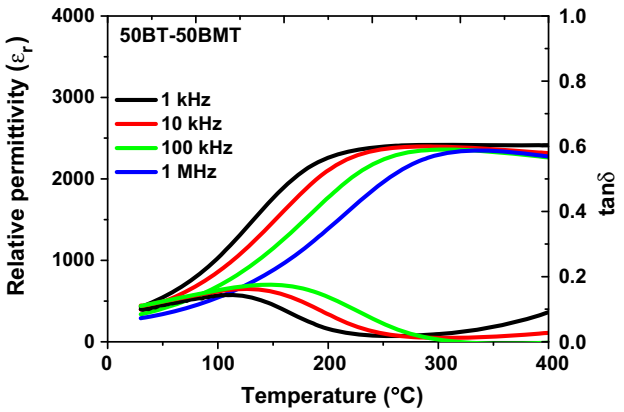

Fig. 3 Relative permittivity, ε_r, and tan δ plot for (1 − x)$BaTiO_3$–x$Bi(Mg_{0.5}Ti_{0.5})O_3$: x = 0.5 fabricated in our laboratory after Ref [23] (Color figure online)

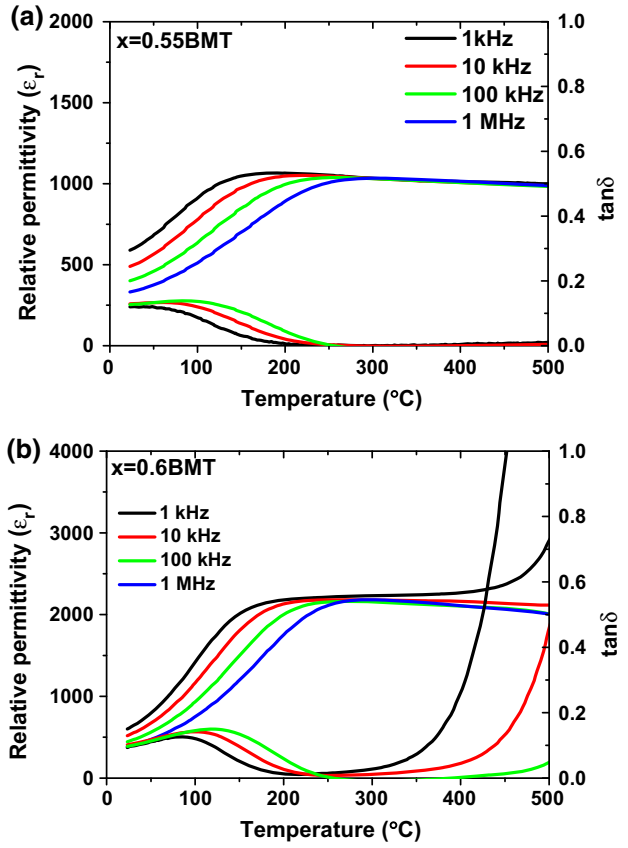

Fig. 4 Relative permittivity ε_r and tan δ versus temperature for (1 − x)$Ba_{0.8}Ca_{0.2}TiO_3$–x$Bi(Mg_{0.5}Ti_{0.5})O_3$ system at **a** x = 0.55, and **b** x = 0.6 [16] (Color figure online)

Expressing temperature stability as TCε_r, the optimum BCT-BMT compositions exhibit TCε_r of $\sim$200 ppm/ °C (where TC$\varepsilon_r = 1/\varepsilon_{r\ mid}[(\varepsilon_{r1}-\varepsilon_{r2})/(T_1-T_2)]$. The materials with optimum dielectric properties have high resistivity: $\sim 10^{10}$ Ω m at 250 °C and 10^7 Ω m at 400 °C.

Increasing the BMT content to x = 0.6 resulted in a minor second phase in XRD patterns, attributed to bismuth titanate. There was also a decrease in resistivity to 10^8 Ω m at 250 °C and 10^6 Ω m at 400 °C, giving higher apparent values of $\varepsilon_{r\ mid} = 2100 \pm 10$ % in the temperature range of 140–420 °C: tan δ ≤ 0.025 from 170 to 300 °C, Fig. 4b [16]. The changeover in properties and increased conductivity at x = 0.6 is thought to be linked to a different defect structure relative to x ≤ 0.55 compositions.

A similar temperature stable dielectric response, but over a narrower temperature range to the optimum $Ba_{0.8}Ca_{0.2}TiO_3$–$Bi(Mg_{0.5}Ti_{0.5})O_3$ samples, was reported for Ca and Zr co-modified compositions. The incorporation of 15 mol% Ca^{2+} allied to 10 mol % Zr substitution, in the solid solution series, $(1-x)Ba_{0.85}Ca_{0.15}Zr_{0.1}Ti_{0.9}O_3$–$xBi(Mg_{0.5}Ti_{0.5})O_3$, resulted in $\varepsilon_{r\ mid} \sim 1200$ from 100 to 350 °C, with tan δ ≤ 0.025 from 150 to 350 °C for x = 0.5 and 0.6 (estimated from published plots) [30]. The corresponding ε_r–T plot for a $(1-x)Ba_{0.85}Ca_{0.15}Zr_{0.1}Ti_{0.9}O_3$–$xBi(Mg_{0.5}Ti_{0.5})O_3$ ceramic of composition $x = 0.6$ prepared in our laboratory is shown in Fig. 5: $\varepsilon_{r\ mid} \sim 1100 \pm 15$ % from 70 to 500 °C, with tan δ ≤ 0.02 from 125 to 480 °C (Fig. 6).

2.4 $Ba_{0.6}Sr_{0.4}Zr_{0.2}Ti_{0.8}O_3$–$Bi(Mg_{0.5}Ti_{0.5})O_3$

Temperature-stable relative permittivity varying by no more than 15 % over wide temperature ranges was observed for $(1-x)Ba_{0.6}Sr_{0.4}Zr_{0.2}Ti_{0.8}O_3$–$xBi(Mg_{0.5}Ti_{0.5})O_3$ ceramics. Composition x = 0.2 gave

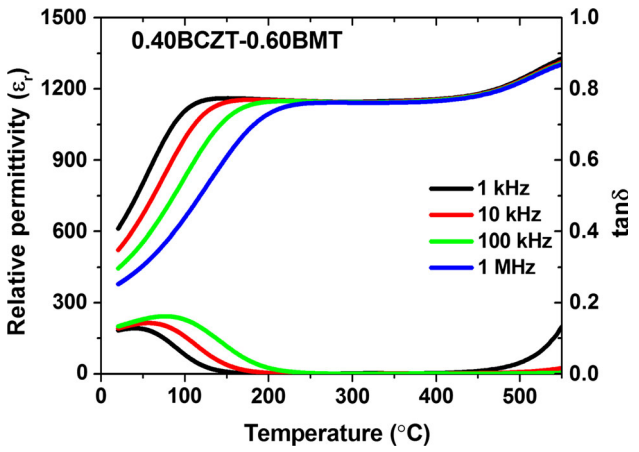

Fig. 5 Relative permittivity, ε_r, and tan δ plot for $0.4Ba_{0.85}Ca_{0.15}Zr_{0.1}Ti_{0.9}O_3$–$0.6Bi(Mg_{0.5}Ti_{0.5})O_3$ fabricated in our laboratory after Ref [30] (Color figure online)

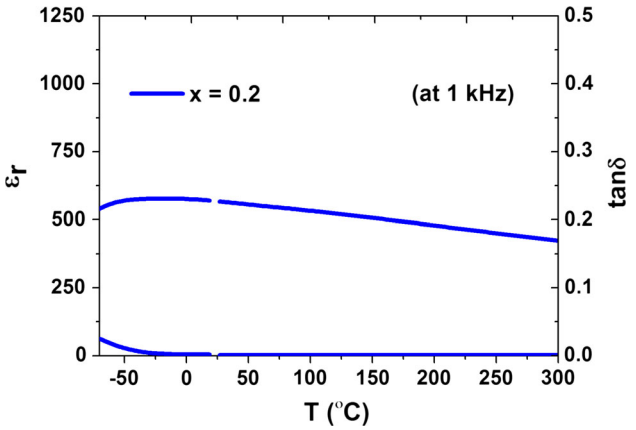

Fig. 6 Relative permittivity ε_r and tan δ plots for $(1-x)Ba_{0.6}Sr_{0.4}Zr_{0.2}Ti_{0.8}O_3$–$xBi(Mg_{0.5}Ti_{0.5})O_3$ x = 0.2. [31] (Color figure online)

$\varepsilon_{r\ mid} = 500 \pm 15$ % from −70 to 300 °C, with tan δ < 0.02 from −60 to 300 °C, Fig. 6 [31]. This matches the target −55–300 °C specification in terms of both stable ε_r and low dielectric loss.

2.5 $Ba_{0.8}Ca_{0.2}TiO_3$–$Bi(Mg_{0.5}Ti_{0.5})O_3$-$NaNbO_3$

A study of $0.45Ba_{0.8}Ca_{0.2}TiO_3$–$(0.55-x)[Bi(Mg_{0.5}Ti_{0.5})O_3$–$xNaNbO_3]$ ceramic compositions (x = 0–0.3) led to a material in which the lower limit of ±15 % stability in ε_r was shifted to sub-zero temperatures, as compared to the parent BCT-BMT system [16, 17, 29]. Incorporation of $NaNbO_3$ at x = 0.2 decreased T_m to 0 °C, from 160 °C in the unmodified material, Fig. 7. The composition x = 0.2 gave $\varepsilon_{r\ mid} = 600 \pm 15$ % in the temperature range −70 to 500 °C, and tan δ ≤ 0.02 from −20 to 400 °C. Further incorporation of $NaNbO_3$ to x = 0.3 in the solid solution decreased T_m to −55 °C with $\varepsilon_{r\ mid} = 550 \pm 15$ % in the temperature range −70 to 300 °C, and tan δ ≤ 0.02 from −60 to 300 °C, again meeting the desire for stability to −55 °C, but at the expense of decreases in ε_r. Values of dc resistivity were in the range $\sim 10^{10}$ Ω m at 250 °C and $\sim 10^7$ Ω m at 400 °C with RC time constant 3–4 s (300 °C).

2.6 $BaTiO_3$–$Bi(Zn_{0.5}Ti_{0.5})O_3$

The $(1-x)BaTiO_3$–$xBi(Zn_{0.5}Ti_{0.5})O_3$ system, BT–BZT, was studied by Huang and Cann [32] at Oregon State University, who determined the solid solution limit to occur at x = 0.33BZT. The crystal system changed from tetragonal for x < 0.1 to mixed tetragonal and rhombohedral at x ∼ 0.1. The ferroelectric Curie peak became broad at x = 0.05, T_c decreased relative to BT, and the lower temperature ε_r discontinuities due to tetragonal-orthorhombic-rhombohedral polymorphic phase transitions

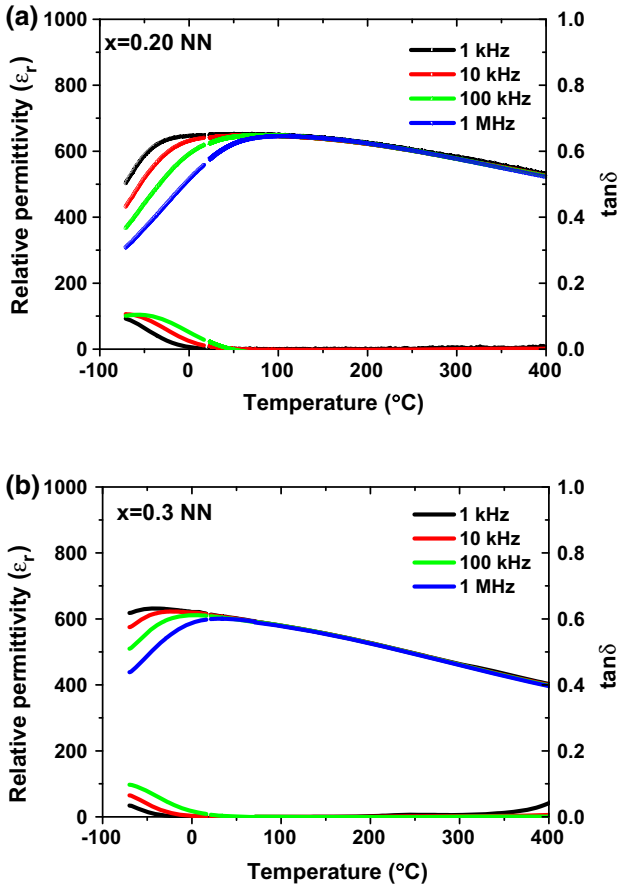

Fig. 7 Relative permittivity ε_r and tan δ for $0.45Ba_{0.8}Ca_{0.2}TiO_3$–$(0.55 - x)Bi(Mg_{0.5}Ti_{0.5})O_3$–$xNaNbO_3$, **a** x = 0.2, and **b** x = 0.3 [17, 29] (Color figure online)

disappeared. Further increases in the BZT content caused dielectric peaks to become increasingly diffuse, and relaxor behaviour was reported at x = 0.2BZT.

A subsequent study by Raengthon and Cann [33] investigated the effect of introducing Ba vacancies (2–8 mol%) into 0.8BT–0.2BZT ceramics. Composition with 2 mol% Ba-deficiency were summised to give improved temperature stability of ε_r, with a nearly flat response from temperatures of 100–350 °C. Designing compositions with Ba vacancies also increased electrical resistivity: the optimum x = 0.2BZT composition (2 mol% Ba deficient) resistivity was of the order of $\sim 7 \times 10^{10}$ Ω cm at 270 °C, decreasing to 5.78×10^9 Ω cm at 335 °C and with a RC time constant of 1.47 s (335 °C). The same research group have proceeded to further characterise BT–BZT ceramics. Incorporating Zr and Mn excess into the BT–BZT based system gave no significant improvements in temperature stability [33]. The group also reported the $(1 - x)[0.5BaTiO_3–0.5Bi(Zn_{0.5}Ti_{0.5})O_3]–xK_{0.5}Bi_{0.5}TiO_3$ system: a relatively stable dielectric response was found for composition x = 0.6KBT. Approximate values (estimated by interpolation of published diagrams) were $\varepsilon_{r\,mid} \sim 2400 \pm 15$ % in the temperature range from 150 to 450 °C with tan δ ~ 0.02 from 200 to 350 °C [34]. Hao et al. [35] have explored core shell structures in doped BT–BZT ceramics fabricated using powders produced by precipitation and by sol–gel methods.

2.7 $BaTiO_3$–$Bi(Zn_{1/2}Ti_{1/2})O_3$–$BiInO_3$

A dielectric study of the $(1 - x)[0.5Bi(Zn_{1/2}Ti_{1/2})O_3–0.5BiInO_3]$-$xBaTiO_3$ ceramic system conducted by Raengthon and Cann [36] revealed a broad and temperature stable dielectric response for compositions x = 0.75 and 0.8. The estimated values interpolated from published plots for composition x = 0.75 were, $\varepsilon_{r\,mid} \sim 1050 \pm 15$ % from 20 to 500 °C with tan δ ≤ 0.05 from 50 to 390 °C. Incorporation of Ba-vacancies (2 mol%) led to decrease of tan δ from 0.184 to 0.008 at 400 °C.

2.8 $BaTiO_3$–$Bi(Zn_{0.5}Ti_{0.5})O_3$–$BiScO_3$

The incorporation of $BiScO_3$ into the BT-BZT system further flattens the ε_r(T) response [37]. The solid solution composition, $50BaTiO_3–25Bi(Zn_{0.5}Ti_{0.5})O_3–25BiScO_3$, compositionally engineered to have 2 mol% Ba-deficiency exhibited $\varepsilon_r \sim 1100$ from 80 to 500 °C (estimated from published plot) with a temperature coefficient of permittivity $TC\varepsilon_r = -182$ ppm/ °C [37], which corresponds to 5 % variation (estimated). Dielectric losses were low, with tan δ = 0.007 at 335 °C. An example of the properties of $50BaTiO_3–25Bi(Zn_{0.5}Ti_{0.5})O_3–25BiScO_3$ ceramic (with 2 mol% Ba deficiency) fabricated in our laboratory is shown in Fig. 8. This material, along with BCT–BMT, x ~ 0.5, developed later in Leeds (Fig. 4a), exhibits the widest temperature ranges of stable ε_r and low tan δ of any material being considered as a high temperature, high permittivity dielectric. However a disadvantage of this material lies in the very high costs of Sc_2O_3. Electrical resistivity reported by Raengthon et al., was 4.1×10^9 Ω cm at 335 °C, higher than for BCT–BMT ceramics.

2.9 $BaTiO_3$–$Bi(Zn_{0.5}Ti_{0.5})O_3$–$NaNbO_3$

Raengthon et al., found that incorporation of small amounts of $NaNbO_3$ into $BaTiO_3–Bi(Zn_{0.5}Ti_{0.5})O_3$ (BT–BZT) according to a compositional formula expressed in mol% terms as, $70BaTiO_3–(30\text{-}y)Bi(Zn_{0.5}Ti_{0.5})O_3–yNaNbO_3$, y = 5–25 shifted T_m to lower temperatures, thereby decreasing the lower temperature limit of stable ε_r to −103 °C from a value of ~100 °C without $NaNbO_3$ modification [32, 38]. Dielectric properties (ε_r–T plots) were shown from −150 to +200 °C: a number of $NaNbO_3$ modified compositions e.g. $70BaTiO_3–5Bi(Zn_{0.5}Ti_{0.5})O_3–25NaNbO_3$ displayed a temperature range of stable ε_r better than X9R (−55–175 °C). The average ε_r values fell from

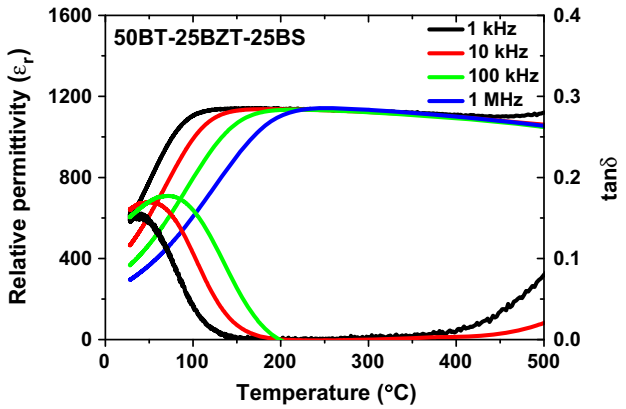

Fig. 8 Relative permittivity ε_r and tan δ versus temperature for $50BaTiO_3$–$25Bi(Zn_{0.5}Ti_{0.5})O_3$–$25BiScO_3$ ceramic with 2 mol% Ba deficiency (fabricated in our laboratory after Ref [36]) (Color figure online)

~1500 in BT–BZT to ≤700 for the $NaNbO_3$ modified compositions with the best low-temperature performance.

2.10 $Ba_{0.8}Ca_{0.2}TiO_3$–$Bi(Zn_{0.5}Ti_{0.5})O_3$

Zeb and Milne investigated the dielectric and ferroelectric properties of $(1-x)Ba_{0.8}Ca_{0.2}TiO_3$–$xBi(Zn_{0.5}Ti_{0.5})O_3$: a nearly flat dielectric response was obtained for $x = 0.3$ with relative permittivity, $\varepsilon_r = 1030 \pm 15$ % over temperatures from ≤25 to 425 °C, with tan $\delta \leq 0.025$ in the temperature range 85–460 °C [39]. The dc resistivity was 10^9 Ω m at a temperature of 300 °C for $x = 0.3$, Fig. 9.

2.11 $BaTiO_3$–$Bi(Zn_{0.5}Zr_{0.5})O_3$

The dielectric properties of $(1-x)BaTiO_3$–$xBi(Zn_{0.5}Zr_{0.5})O_3$ [BT–xBZZ] were studied by Wang et al. [40]. Increasing the BZZ content induced relaxor behaviour in ε_r–T plots, with supressed values of $\varepsilon_{r\ max}$. Good temperature stability in ε_r was reported for $x = 0.6$, with $\varepsilon_{r\ mid} = 1000 \pm 15$ % from 200 to 450 °C, with tan $\delta \leq 0.25$ from room temperature to 300 °C (estimated).

2.12 $BaTiO_3$–$Bi(Mg_{0.5}Zr_{0.5})O_3$

Zeb and Milne [41] demonstrated stability in relative permittivity in the ceramic system $(1-x)BaTiO_3$–$xBi(Mg_{0.5}Zr_{0.5})O_3$, BT–xBMZ. The end member BT ($x = 0$) changed from tetragonal to pseudocubic phase at $x \geq 0.1$BMZ; a single phase solid solution was obtained for $x < 0.5$BMZ. The $x = 0.03$ and 0.05BMZ compositions exhibited double peaks in ε_r–T plots which correlated to core–shell grain structures, as confirmed by TEM analysis. However composition $x = 0.3$BMZ gave a stable dielectric response, with $\varepsilon_{r\ mid} = 570 \pm 15$ % from −20 to 430 °C, and tan $\delta \leq 0.02$ from 30 to 420 °C, Fig. 10. Composition $x = 0.4$BMZ gave $\varepsilon_{r\ mid} = 600 \pm 15$ % from 25 to 420 °C with tan $\delta \leq 0.02$ from 55 to 280 °C, Fig. 10. Values of dc resistivity were 10^9 Ω m at 250 °C, and 10^6 Ω m at 400 °C.

2.13 $BaTiO_3$–$Bi(Mg_{2/3}Nb_{1/3})O_3$

Wang et al. [42] examined the solid solution, $(1-x)BaTiO_3$–$xBi(Mg_{2/3}Nb_{1/3})O_3$, reporting basic dielectric properties and energy storage capabilities. Composition $x = 0.2$ exhibited temperature-stable dielectric response with ε_r varying from 628 to 787 in the temperature range −50 to +300 °C: tan $\delta \leq 0.025$ over the temperature range 0–150 °C (estimated). Values of dc resistivity were of 7.4×10^{12} Ω cm at room temperature and energy density of 0.74 J/cm^3 (160 kV/cm) was recorded for $x = 0.2$. However, all compositions of this system showed a sharp increase in dielectric loss tangent at temperature ≥200 °C.

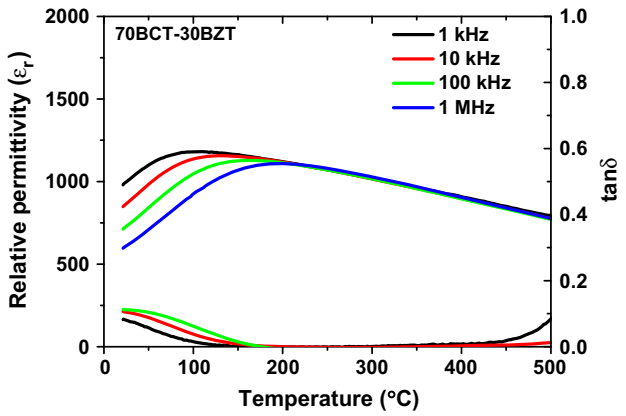

Fig. 9 Relative permittivity ε_r and tan δ plot for $(1-x)Ba_{0.8}Ca_{0.2}TiO_3$–$xBi(Zn_{0.5}Ti_{0.5})O_3$: $x = 0.3$ [38] (Color figure online)

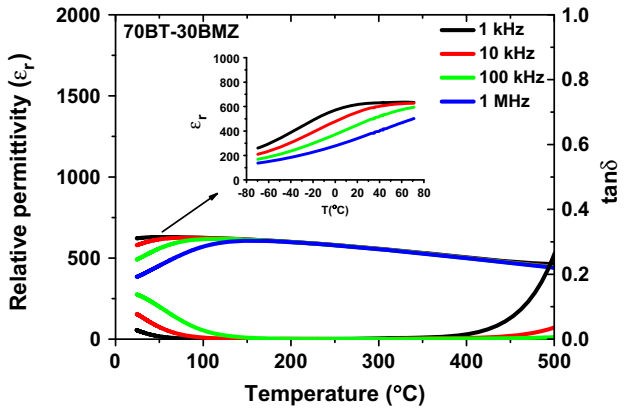

Fig. 10 Relative permittivity, ε_r, and tan δ plot for $(1-x)BaTiO_3$–$xBi(Mg_{0.5}Zr_{0.5})O_3$: $x = 0.3$ (inset shows ε_r from temperature −70 to +70 °C) [40] (Color figure online)

2.14 $BaTiO_3$–$Bi(Mg_{2/3}Ta_{1/3})O_3$

Ma et al. [43] studied the dielectric properties of the $(1 - x)BaTiO_3$–$xBi(Mg_{2/3}Ta_{1/3})O_3$ ceramic system. Composition $x = 0.1$ exhibited dielectric stability across the temperature range 30–150 °C, with $\varepsilon_{r\ max} = 1278$: $\tan\delta \leq 0.02$ over the temperature range 30–195 °C. There was a sharp rise in dielectric loss tangent at a temperature of ≥200 °C.

2.15 $BaTiO_3$–$BiAlO_3$

Liu et al. [44] fabricated the binary $(1 - x)BaTiO_3$–$xBiAlO_3$ ceramic system by solid state and sol–gel processing routes. The temperature stability in ε_r–T plots increased with increases in the $BiAlO_3$ content. The best temperature stability in ε_r was demonstrated for ceramic samples fabricated using powders prepared by the sol–gel method. At $x = 0.3BiAlO_3$, $\varepsilon_{r\ max} = 660 \pm 15$ % over the temperature range −55–440 °C: $\tan\delta \sim 0.012$ at room temperature. However, conventional solid state methods for producing the starting powders failed to achieve this level of temperature range of stability. The reported relative permittivity for the solid state route for composition $x = 0.3$ was $\varepsilon_r = 1558 \pm 15$ % across the temperature range, −55–124 °C. These researchers also studied the effect of Nb incorporation to $0.8BaTiO_3$–$0.2BiAlO_3$ ($x = 0.2$) to try to extend the working temperature range. A sample composition containing 4 mol% Nb displayed $\varepsilon_r = 925 \pm 15$ % from −55 to 178 °C, and $\tan\delta \sim 0.004$ in the temperature range −20–200 °C (estimated).

A summary of properties of selected $BaTiO_3$ and $Bi_{0.5}Na_{0.5}TiO_3$ based materials is presented in Table 2.

3 $Na_{0.5}Bi_{0.5}TiO_3$-based materials

3.1 $Na_{0.5}Bi_{0.5}TiO_3$–$NaNbO_3$

The system $(1 - x)Na_{0.5}Bi_{0.5}TiO_3$–$xNaNbO_3$ (NBT–NN) was investigated for $NaNbO_3$ contents up to $x = 0.08$ [45]. The NBT end-member is a relaxor dielectric with a broad ε_r peak at ~300 °C, and shoulder at ~180 °C. Incorporation of $NaNbO_3$ in the range $x = 0.01$–0.03 shifts the peak and shoulder to lower temperatures; both features become increasingly diffuse for $NaNbO_3$ modified samples [45]. At $x = 0.08$, a broad ε_r(T) plateau extends from ~200 to 400 °C but with continued evidence of two distinct humps.

Bridger et al. [46] patented a series of high temperature dielectric materials based on the relaxor sodium bismuth titanate (NBT). A a variety of substituents and dopants were used to broaden and adjust the temperature of the ε_r(T) shoulder and main peak. Example minor substituents included Sr, Ca, Ba: a further flattening of the dielectric response was achieved, along with increases in electrical resistivity, through the use of dopants (Mn, Cu, Co). In agreement with earlier work by Li et al. [45], the binary solid solution between $Na_{0.5}Bi_{0.5}TiO_3$ and $NaNbO_3$ displayed a flattened dielectric response over a wide temperature range [46]. Optimum compositions gave $\varepsilon_r > 1000$, and $\tan\delta < 0.02$ over the temperature range −30 to +200 °C: resistivity was $>10^{10}$ Ω m. The wide variety of compositions described in the 2008 Bridger patent application, with full patent granted in 2010, can be grouped into two categories depending on the temperature range of stable dielectric response: (a) compositions with stable properties from <0 to +200 °C; (b) higher temperature dielectrics with stability from a minimum temperature 200 ± 100 °C to an upper limit 400 ± 100 °C. Certain dopants increased resistivity and improved voltage coefficients to within ±20 % (or in some cases ±10 %) for electric fields up to 10 MV/m [46, 47]. Specific examples of the main NBT parent compositions reported by Bridger et al., and their dielectric properties are presented in summary Table 2.

3.2 $Na_{0.5}Bi_{0.5}TiO_3$–$KTaO_3$

König et al. [48] reported trends in ε_r(T) peak temperatures and widths of ε_r peaks of various $(1 - x)Na_{0.5}Bi_{0.5}TiO_3$–$xKTaO_3$ binary compositions. Increasing the $KTaO_3$ content resulted in a fatter ε_r-T response: for composition $x = 0.2$, $\varepsilon_{r\ mid} = 2000 \pm 15$ %, in the temperature range 80–300 °C (estimated) with $\tan\delta \leq 0.02$ over a narrower temperature range, from 200 to 300 °C. For composition $x = 0.05$ annealed at high temperatures, a broad dielectric maxima $\varepsilon_{r\ max} = 2700$, from 160 to 260 °C with $\tan\delta \leq 0.02$ was reported spanning temperatures from 100 to 300 °C (estimated).

3.3 $Na_{0.5}Bi_{0.5}TiO_3$–$BaTiO_3$–$K_{0.5}Na_{0.5}NbO_3$

Dittmer et al. Technical University Darmstadt, studied the ternary system, $(1 - x)(0.94Na_{0.5}Bi_{0.5}TiO_3$–$0.06BaTiO_3)$–$xK_{0.5}Na_{0.5}NbO_3$, [NBT–BT–KNN] for compositions $x \leq 0.18$ KNN [49]. In a similar manner to NBT-based materials reported by Li et al., for the $Na_{0.5}Bi_{0.5}TiO_3$–$NaNbO_3$ system, and by Bridger et al., for complex compositions based on NBT [45, 46]. Dittmer et al., observed a ε_r(T) plateau which exhibited two broad humps originating from the shoulder and broad ε_r peak in the base material. However the width of the ε_r-T plateau was greater in the NBT-BT-KNN system. Optimum properties occurred at $x = 0.18$KNN, with $\varepsilon_r = 2151 \pm 10$ %, from temperatures of 43 to 319 °C: $\tan\delta \leq 0.025$ from ~50 to <300 °C

(estimated from published plot). For NBT-BT-KNN at x = 0.18, electrical resistivity was 10^8 Ω m at 300 °C, and RC time constant ~1.13 s. For x = 0.15, the reported properties were, $\varepsilon_r = 2349 \pm 10$ % from 49 to 313 °C, with tan δ ≤ 0.025 from ~100 to 300 °C (estimated).

3.4 $Na_{0.5}Bi_{0.5}TiO_3$–$K_{0.5}Bi_{0.5}TiO_3$–$K_{0.5}Na_{0.5}NbO_3$

The Darmstadt group subsequently studied (1 − x)[0.6$Na_{0.5}Bi_{0.5}TiO_3$–0.4$K_{0.5}Bi_{0.5}TiO_3$]–x$K_{0.5}Na_{0.5}NbO_3$, x = 0.08–0.015 ceramics, reporting $\varepsilon_r = 2167 \pm 10$ %, from 54 to 400 °C for the best composition, x = 0.15KNN. In compositions with the widest temperature range of stability in ε_r, namely x = 0.12 and 0.15 KNN, tan δ < 0.025 (1 kHz) over what appeared to be a temperature span, ~100–250 °C (estimated) compared to ε_r stability over a broader temperature range, 54–400 °C [50].

There is some evidence from published data that dielectric losses in NBT–KBT–KNN show a greater temperature fluctuation than for the leading $BaTiO_3$–$Bi(Mg_{0.5}Ti_{0.5})O_3$ or $BaTiO_3$–$Bi(Zn_{0.5}Ti_{0.5})O_3$ based dielectric ceramics, and in NBT–KBT–KNN low loss occurs over a significantly narrower temperature range than the full range of the ε_r plateau. However a full comparison of ceramics of the different leading systems prepared on one laboratory would be required to verify this observation and to confirm working temperature ranges in terms of ε_r stability and low loss.

The effect of incorporating $CaZrO_3$ into NBT–BT and NBT–BT–KNN was to decrease the lower operating temperature and also to decrease ε_r values [51, 52]. The materials were prepared according to solid solution formulae: (1 − x)[0.94$Na_{0.5}Bi_{0.5}TiO_3$–0.06$BaTiO_3$]–x$CaZrO_3$ and (1 − x)[0.82(0.94$Na_{0.5}Bi_{0.5}TiO_3$–0.06$BaTiO_3$)–0.18$K_{0.5}Na_{0.5}NbO_3$]–x$CaZrO_3$ respectively. Ceramics with different $CaZrO_3$ [CZ] contents exhibited different combinations of $\varepsilon_{r\,max}$ and plateau temperature ranges. For the NBT–BT–CZ compositional series, the lower limiting temperature of near flat ε_r(T) decreased with increasing amounts of $CaZrO_3$ substitution, from 109 °C at 0.05CZ to −97 °C at 0.2CZ. For NBT–BT–KNN–CZ solid solutions, the variation was from −6 to −69 °C with increasing levels of $CaZrO_3$ incorporation. Dielectric losses (1 kHz) increased sharply at temperatures above 200–300 °C in both NBT–BT–CZ and NBT–BT–KNN–CZ. The NBT–BT–CZ composition x = 0.2CaZrO_3 gave the flattest ε_r-T response, with a ± 15 % consistency in ε_r (550 mean) from −97 to +371 °C, with tan δ = 0.7 % at 300 °C (1 kHz). Dielectric losses (deduced from ε''-T plots) increased substantially above 300 °C, suggesting a practical upper working temperature (combination of stable ε_r and low loss) may be ~300 °C.

In the NBT–BT–KNN–CZ system, the flattest ε_r–T response again occurred for x = 0.2CZ [51]. In this case, the temperature range of ±15 % consistency in ε_r (467 mean) extended from −69 to +468 °C; dielectric loss at 1 kHz (tan $\delta = \varepsilon_r''/\varepsilon_r'$) increased sharply above 300 °C. An electrical resistivity of ~10^7 Ω m at 300 °C was recorded for the BNT–BT–CZ composition x = 0.2 which had the most stable dielectric properties. For the BNT–BT–KNN–CZ compositions, the electrical resistivity was ~10^8 Ω m at 300 °C for x = 0.2CZ: other compositions with less favourable ε_r-T response exhibited higher resistivity, up to 10^9 Ω m (e.g. BNT–BT–KNN–0.05 CZ).

3.5 $Bi_{0.5}Na_{0.5}TiO_3$–$BaTiO_3$–$Bi_{0.2}Sr_{0.7}TiO_3$

Shi et al. reported the electrical properties for the Bi-deficient solid solution series '$(Bi_{0.5-y}Na_{0.5})_{0.94-x}Ba_{0.06}(Bi_{0.2}Sr_{0.7}\square_{0.1})_xTiO_3$' derived from a BNT–BT composition at its morphotropic phase boundary [53]. The system demonstrated promising temperature stable dielectric properties with low loss tangent. A flat dielectric response with very high relative permittivity, $\varepsilon_r = 4884 \pm 10$ % was reported for composition x = 0.26, y = 0.07 over the temperature span 50–270 °C: tan δ ≤ 0.02 from 100 to 300 °C (estimated). A rapid decrease in ε_r occurred for temperatures outside this range. The value of time constant (RC) was 5.96 s at a temperature of 300 °C.

4 Other materials

4.1 $BiScO_3$–$BaTiO_3$–$(K_{1/2}Bi_{1/2})TiO_3$

Lim et al. investigated the ternary (1 − x)[0.4$BiScO_3$–0.6$BaTiO_3$]–x$K_{0.5}Bi_{0.5}TiO_3$ series [54]. The x = 0.2KBT material displayed a temperature-insensitive response with $\varepsilon_{r\,max} = 1750$, and $TC\varepsilon_r = -800$ ppm/ °C across the temperature range 200–400 °C: tan δ < 0.02 for the equivalent temperature range. The energy density increased from 0.3 J/cm^3 at 50 kV/cm to 4.0 J/cm^3 at 220 kV/cm. An electrical resistivity of 10^9 Ω cm and RC constant 0.8 s at 300 °C were reported.

4.2 $K_{0.5}Bi_{0.5}TiO_3$–$BiScO_3$

Kruea-In et al. [18] reported temperature-insensitive dielectric properties in the (1 − x)$K_{0.5}Bi_{0.5}TiO_3$–x$BiScO_3$, KBT–BS relaxor system. Compositions x = 0.15BS and x = 0.2BS presented flat ε_r–T responses: for example x = 0.15 exhibited a ±3 % variation in relative permittivity about $\varepsilon_{r\,mid} = 2880$ across the temperature range 227–427 °C. Independently Martín-Arias et al., reported a similar temperature stable dielectric response for composition x = 0.2 [55].

4.3 $K_{0.5}Na_{0.5}NbO_3$–$LiTaO_3$

Another approach to achieving wide-ranging temperature stability is not reliant on relaxor behaviour. Instead ferroelectrics with high T_c offer stable properties below Tc, albeit with moderate ε_r values. This is illustrated by the $(1-x)K_{0.5}Na_{0.5}NbO_3$–$xLiTaO_3$ solid solution series [KNN–LT], taking advantage of the high ferroelectric Curie temperature of NKN ($T_c \sim 420$ °C). Unmodified NKN displays an orthorhombic ↔ tetragonal polymorphic phase transition at ~200 °C creating a ε_r discontinuity which prevents temperature stability in ε_r values at $T < T_c$. This transition can be shifted to much lower temperatures through appropriate levels of $LiTaO_3$ incorporation, Fig. 11, as demonstrated by Skidmore et al. [56, 57]. The polymorphic phase transition can be shifted to below 0 °C by incorporation of between 0.7LT and 0.1LT, thereby imparting improved temperature stability. A flat ε_r–T response was obtained for $x = 0.1LiTaO_3$ from temperatures −50 to 350 °C with $\varepsilon_r \sim 480 \pm 15$ %: the upper temperature limit lies at the onset of the tail to the ferroelectric Curie peak ($T_c \sim 450$ °C) [56]. For the composition $x = 0.07$, a slightly narrower temperature-stable range occurred, with $\varepsilon_r = 630$–700 ± 15 % from −15 to +300 °C [56, 58].

4.4 $Na_{0.5}K_{0.5}NbO_3$–$LiTaO_3$–$BiScO_3$

Skidmore et al. [59] studied dielectric and piezoelectric properties in the ternary compositional system $(1-x)[(Na_{0.5}K_{0.5}NbO_3)_{0.93}$–$(LiTaO_3)_{0.07}]$–$xBiScO_3$. Addition of $BiScO_3$ led to a decrease in values of $\varepsilon_{r\,max}$ from ~3600 at $x = 0$ to ~1800 at $x = 0.02$ and the creation of a diffuse ε_r–T peak. The dielectric response become flatter at $x = 0.05$ with estimated ε_r values of ~1150 ± 15 % from ~20 to 450 °C [56, 59]: tan δ values were 0.03–0.05 for temperatures from 20 to 200 °C, decreasing to <0.025 at 200–350 °C [56].

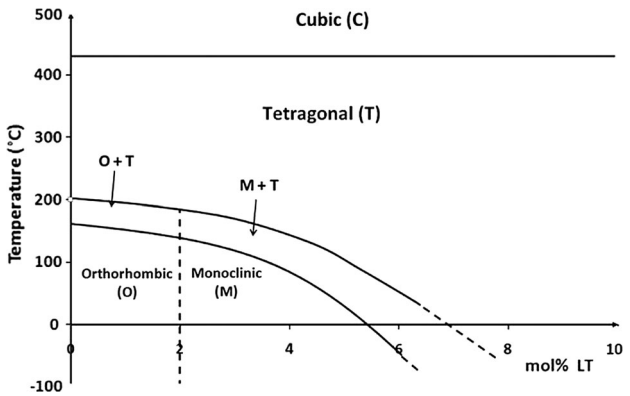

Fig. 11 Phase diagram for the $Na_{0.5}K_{0.5}NbO_3$–$LiTaO_3$ system [56]

Zhu et al., studied dielectric and piezoelectric properties in the system, $(1-x)[0.98Na_{0.5}K_{0.5}NbO_3$–$0.02BiScO_3]$–$xLiTaO_3$ [60, 61]. Values of $\varepsilon_{r\,max}$ decreased from an estimated 7000 at $x = 0$, to 2600 at $x = 0.03LiTaO_3$. Composition $x = 0.02$ $LiTaO_3$ showed consistent $\varepsilon_r(T)$ response with ε_r estimated at 1000 ± 15 % from 0 to 300 °C. The $x = 0.03$ samples gave $\varepsilon_r \sim 700 \pm 15$ % from approximately −55–200 °C. Values of tan δ were ~0.03 over these temperature ranges. For certain compositions, the broad ε_r–T response showed two sub-peaks. Analysis by TEM-EDX indicated the origin of the sub-peaks in certain $Na_{0.5}K_{0.5}NbO_3$–$LiTaO_3$–$BiScO_3$ compositions, e.g. $0.98[0.95Na_{0.5}K_{0.5}NbO_3$–$0.05LiTaO_3]$–$0.02BiScO_3]$, was due to core–shell segregation [62].

4.5 $K_{0.5}Na_{0.5}NbO_3$–$Bi(Zn_{0.75}W_{0.25})O_3$

The solid solution $(1-x)K_{0.5}Na_{0.5}NbO_3$–$xBi(Zn_{0.75}W_{0.25})O_3$, [KNN–BZW] was synthesised by Chen et al. [63]. The crystal structure was identified as having orthorhombic symmetry with no evidence of secondary phases. Plots of ε_r–T indicated two phase transitions above room temperature: orthorhombic-tetragonal and tetragonal-cubic. These transitions became more diffuse with increasing BZW content. Composition $x = 0.01$BZW gave temperature- stable dielectric behaviour, with $\varepsilon_r \sim 1300 \pm 15$ % from temperatures of 150–350 °C; tan $\delta < 0.04$ across this temperature range.

5 Summary

A wide variety of compositionally complex perovskite solid solutions display near-stable relative permittivity over wide temperature ranges with upper temperature limits of stable ε_r (±15 %) of 300–500 °C. The properties of the most

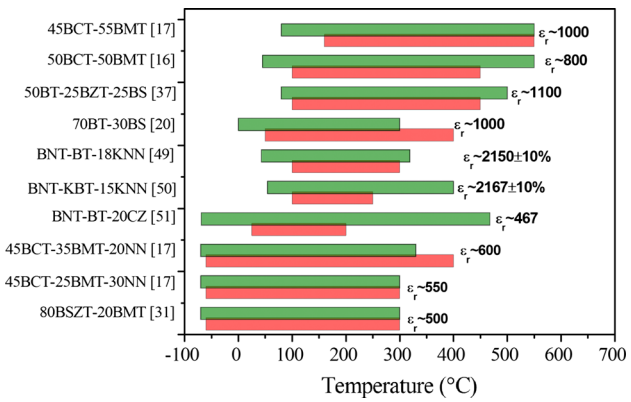

Fig. 12 Bar plots representing temperature range of ±15 % or better stability of ε_r (*green bars*): range of low tan $\delta < 0.02$ represented by *red bars* (Color figure online)

promising materials are summarised in Table 2; a graphical comparison of the best materials is shown in Fig. 12. The materials with the widest temperature range of stable and high relative permittivity ($\varepsilon_r \sim 1000$), low dielectric loss and high electrical resistivity in a single material are found in the $Ba_{0.8}Ca_{0.2}TiO_3$–$Bi(Mg_{0.5}Ti_{0.5})O_3$ and $BaTiO_3$–$Bi(Zn_{0.5}Ti_{0.5})O_3$–$BiScO_3$ systems. However the lower temperature limit lies above room-temperature for these materials, which is restrictive for capacitor applications. Other materials which do achieve stability down to −55 °C exhibit moderate relative permittivity values ($\varepsilon_r \sim 500$). Therefore despite the advances in high temperature dielectric ceramics reviewed in this paper, further improvements in basic dielectric properties and working temperature ranges are required to bring the materials to a stage where they can be considered for further evaluation and implementation as practical high temperature capacitor materials. In addition, capacitor-grade testing including voltage stability and dielectric breakdown strength measurements will be required to confirm if a material is suitable for capacitor applications. At the time of writing this review, there is little published information on measurements of breakdown strengths performed according to statistically valid protocols. Ogihara et al. [20] applied a dc field to BT–BS samples of thickness 0.9–0.05 mm (ramp rate 500 V/s) reporting a current spike at 275 ± 39 kV/cm for a 0.48 mm thick sample (7 tested) and 764 ± 52 kV/cm for a 0.05 mm film (6 tested) [20]. In the case of (1 − x)BCT–xBMT, a preliminary study in collaboration with D A Hall at Manchester University indicated electrical breakdown to occur at 258 ± 30 kV/cm for 0.3 mm pellets and 204 ± 14 kV/cm for 0.5 mm pellets (10 tested at room temperature; ramp 500 V/s), but this type of measurement gives only an estimate of breakdown. The same BCT–BMT material (x = 0.55) under dc bias at a temperature of 180° retained a consistent value of relative permittivity of ∼1200 at dc bias fields up to 4 kV/mm. This contrasts to the severe decrease in permittivity of ferroelectric materials under dc bias fields, and suggests temperature stable relaxors have promise in energy storage applications, provided breakdown strengths are sufficient (energy storage varies as $\varepsilon_r E^2$) [64].

Acknowledgments A Zeb wishes to thank the Higher Education of Pakistan and Islamia College Peshawar (Chartered University, KPK) for financial support. We wish to thank Saeed Ullah Jan for providing data for Figure 6 and David A Hall, Manchester University for help with high voltage measurements.

References

1. J. Watson, C. Castro, Analog Dialogue **46**(4), 3–9 (2012)
2. J. Watson, C. Castro, J. Mater. Sci Electron. (2015). doi:10.1007/s10854-015-3459-4
3. R. Phillips, J. Bultitude, A. Gurav, K. Park, S. Murillo, P. Flores, M. Laps, CARTS International 2013 Proceedings, Houston Texas USA (2013)
4. M. Barta, S. Pala, S.P. Cygan. http://www.avx.com/docs/techinfo/Capacitors_high_temp.pdf
5. C.L.H. Zhou et al., IEEE Trans. Circ. Sys. **60**, 542–546 (2013)
6. P.G. Neudeck, R.S. Okojie, L.-Y. Chen, Proc. IEEE **90**(6), 1065–1076 (2002)
7. EU-Directive 2002/96/EC, Off. J. Eur. Union, **46** (L37), 24–38 (2003)
8. EU-Directive 2002/95/EC, Off. J. Eur. Union, **46** (L37), 19–23 (2003)
9. X. Xu, A.S. Gurav, P.M. Lessner, C.A. Randall, Ind. Electron. IEEE Trans. **58**(7), 2636–2643 (2011)
10. G. Smolensky, Ferroelectrics **53**(1), 129–135 (1984)
11. C. Laulhé, F. Hippert, J. Kreisel, M. Maglione, A. Simon, J. Hazemann, V. Nassif, Phys. Rev. B **74**(1), 014106 (2006)
12. V.V. Shvartsman, D.C. Lupascu, J. Am. Ceram. Soc. **95**(1), 1–26 (2012)
13. H.C. Wang, W.A. Schulze, J. Am. Ceram. Soc. **73**(4), 825–832 (1990)
14. A. Bokov, Z.-G. Ye, *Frontiers of Ferroelectricity* (Springer, Berlin, 2007), pp. 31–52
15. A. Zeb, S.J. Milne, J. Am. Ceram. Soc. **96**(10), 3089–3093 (2013)
16. A. Zeb, S.J. Milne, J. Am. Ceram. Soc. **96**(9), 2887–2892 (2013)
17. A. Zeb, Y. Bai, T. Button, S.J. Milne, J. Am. Ceram. Soc. **97**(8), 2479–2483 (2014)
18. C. Kruea-In, G. Rujijanagul, F.Y. Zhu, S.J. Milne, Appl. Phys. Lett. **100**(20), 202904 (2012)
19. C.-C. Huang, D.P. Cann, X. Tan, N. Vittayakorn, J. Appl. Phys. **102**(4), 044103–044103-5 (2007)
20. H. Ogihara, C.A. Randall, S. Trolier-McKinstry, J. Am. Ceram. Soc. **92**(1), 110–118 (2009)
21. Tinberg DS, Trolier-McKinstry S (2007) J Appl Phys 101(2), 024112-1–024112-4
22. S. Wada, K. Yamato, P. Pulpan, N. Kumada, B.-Y. Lee, T. Iijima, C. Moriyoshi, Y. Kuroiwa, J. Appl. Phys. **108**(9), 094114 (2010)
23. Q. Zhang, Z. Li, F. Li, Z. Xu, J. Am. Ceram. Soc. **94**(12), 4335–4339 (2011)
24. D.H. Choi, A. Baker, M. Lanagan, S. Trolier-McKinstry, C. Randall, J. Am. Ceram. Soc. **96**(7), 2197–2202 (2013)
25. B. Xiong, H. Hao, S. Zhang, H. Liu, M. Cao, Z. Yu, Ceram. Int. **38**, S45–S48 (2012)
26. B. Xiong, H. Hao, S. Zhang, H. Liu, M. Cao, J. Am. Ceram. Soc. **94**(10), 3412–3417 (2011)
27. H. Hao, H. Liu, S. Zhang, B. Xiong, X. Shu, Z. Yao, M. Cao, Scr. Mater. **67**(5), 451–454 (2012)
28. D. Hennings, H. Schreinemacher, Mater. Res. Bull. **12**(12), 1221–1226 (1977)
29. A. Zeb, S.J. Milne, J. Am. Ceram. Soc. **96**(12), 3701–3703 (2013)
30. W. Bai, J. Hao, B. Shen, J. Zhai, Ceram. Int. **39**(Supplement 1), S19–S23 (2013)
31. S.U Jan, Ph.D. Thesis, University of Leeds
32. Huang C-C, Cann DP (2008) J. Appl. Phys. 104(2), 024117-1–024117-4
33. N. Raengthon, D.P. Cann, Ultrason Ferroelectr. Freq. Control IEEE Trans. **58**(9), 1954–1958 (2011)
34. A. Prasatkhetragarn, B. Yotburut, N. Triamnak, R. Yimnirun, D.P. Cann, Ceram. Int. **38**(1), 827–830 (2012)
35. H. Hao, M. Liu, H. Liu, S. Zhang, X. Shu, T. Wang, Z. Yao, M. Cao, RSC Adv. **5**(12), 8868–8876 (2015)
36. N. Raengthon, D.P. Cann, J. Electroceram. **28**(2–3), 165–171 (2012)
37. N. Raengthon, T. Sebastian, D. Cumming, I.M. Reaney, D.P. Cann, J. Am. Ceram. Soc. **95**(11), 3554–3561 (2012)

38. N. Raengthon, H.J. Brown-Shaklee, G.L. Brennecka, D.P. Cann, J. Mater. Sci. **48**(5), 2245–2250 (2013)
39. A. Zeb, S.J. Milne, J. Eur. Ceram. Soc. **34**(7), 1727–1732 (2014)
40. Y. Wang, X. Chen, H. Zhou, L. Fang, L. Liu, H. Zhang, J. Alloys Compd. **551**, 365–369 (2013)
41. A. Zeb, S.J. Milne, J. Eur. Ceram. Soc. **34**(13), 3159–3166 (2014)
42. T. Wang, L. Jin, C. Li, Q. Hu, X. Wei, J. Am. Ceram. Soc. **98**(2), 559–566 (2015)
43. D. Ma, X. Chen, G. Huang, J. Chen, H. Zhou, L. Fang, Ceram. Int. **41**(5), 7157–7161 (2015)
44. M. Liu, H. Hao, Y. Zhen, T. Wang, D. Zhou, H. Liu, M. Cao, Z. Yao, J. Eur. Ceram. Soc. **35**(8), 2303–2311 (2015)
45. Y. Li, W. Chen, J. Zhou, Q. Xu, H. Sun, R. Xu, Mater. Sci. Eng. B **112**(1), 5–9 (2004)
46. K. Bridger, A.V. Cooke, W.A. Schulze, US patent 2008/0239627 A1 (2008)
47. K. Bridger, A.V. Cooke, W.A. Schulze, US patent 2010/7697263 B2 (2010)
48. J. König, M. Spreitzer, D. Suvorov, J. Eur. Ceram. Soc. **31**(11), 1987–1995 (2011)
49. R. Dittmer, W. Jo, D. Damjanovic, J. Rödel, J. Appl. Phys. **109**(3), 034107 (2011)
50. R. Dittmer, E.M. Anton, W. Jo, H. Simons, J.E. Daniels, M. Hoffman, J. Pokorny, I.M. Reaney, J. Rödel, J. Am. Ceram. Soc. **95**(11), 3519–3524 (2012)
51. M. Acosta, J. Zang, W. Jo, J. Rödel, J. Eur. Ceram. Soc. **32**(16), 4327–4334 (2012)
52. J. Zang, M. Li, D.C. Sinclair, T. Frömling, W. Jo, J. Rödel, J. Am. Ceram. Soc. **97**(9), 2825–2831 (2014)
53. J. Shi, H. Fan, X. Liu, Y. Ma, Q. Li, J. Alloys Compd. **627**, 463–467 (2015)
54. J.B. Lim, S. Zhang, N. Kim, T.R. Shrout, J. Am. Ceram. Soc. **92**(3), 679–682 (2009)
55. L. Martín-Arias, A. Castro, M. Algueró, J. Mater. Sci. **47**(8), 3729–3740 (2012)
56. T.A. Skidmore, PhD thesis, University of Leeds, UK (2009)
57. T.A. Skidmore, T.P. Comyn, A.J. Bell, F. Zhu, S.J. Milne, Ultrason Ferroelectron. Freq. Control IEEE Trans. **58**(9), 1819–1825 (2011)
58. T.A. Skidmore, T.P. Comyn, S.J. Milne, Appl. Phys. Lett. **94**(22), 222902–222902-3 (2009)
59. T.A. Skidmore, T.P. Comyn, S.J. Milne, J. Am. Ceram. Soc. **93**(3), 624–626 (2010)
60. F. Zhu, T.A. Skidmore, A.J. Bell, T.P. Comyn, C.W. James, M. Ward, S.J. Milne, Mater. Chem. Phys. **129**(1), 411–417 (2011)
61. F. Zhu, M.B. Ward, T.P. Comyn, A.J. Bell, S.J. Milne, Ultrason Ferroelectron. Freq. Control IEEE Trans. **58**(9), 1811–1818 (2011)
62. F. Zhu, M.B. Ward, J.-F. Li, S.J. Milne, Acta Mater. **90**, 204–212 (2015)
63. X. Chen, J. Chen, D. Ma, G. Huang, L. Fang, H. Zhou, Mater. Lett. **145**, 247–249 (2015)
64. X. Hao, J Adv. Dielectr. **3**(1), 1330001 (2013)